Gan, G., and Riffat, S. 1995. k-factors for HVAC ducts: Numerical and experimental determination. *Building Service Engineering Research and Technology* 16(3):133-139.

Gan, G., and Riffat, S. 1997. Pressure loss characteristics of orifice and perforated plates. *Experimental Thermal and Fluid Science* 14(2):160-165.

Germano, M., Piomelli, U., Moin, P., and Cabot, W. 1996. Dynamic subgrid-scale eddy viscosity model. *In Summer Workshop, Center for Turbulence Research, Stanford, CA.*

Gibson, M., and Launder, B. 1978. Ground effects on pressure fluctuations in the atmospheric boundary layer. *Journal of Fluid Mechanics* 86:491-511.

Kulkarni, D., Khaire, S., and Idem, S. 2009. Measurements of flat oval elbow loss coefficients. *ASHRAE Transactions* 115(1):35-47.

Launder, B., and Spalding, D. 1974. The numerical computation of turbulent flows. *Computer Methods in Applied Mechanics and Energy* 3:269-289.

Mahank, T., and Mumma, S. 1997. Flow Modeling of flat oval ductwork elbows using computational fluid dynamics. *ASHRAE Transactions* 103(2):365-374.

Moody, L. 1944. Friction factors for pipe flow. *Transactions of the ASME* 66(8): 671-684.

Mumma, S., Mahank, T., and Ke, Y. 1997. Close coupled ductwork fitting pressure drop. *HVAC&R Research* 3(2): 158-177.

Mumma, S., Mahank, T., and Ke, Y. 1998. Analytical determination of duct fitting loss-coefficients. *Applied Energy* 61: 229-247.

Shao, L., and Riffat, S. 1995. Accuracy of CFD for predicting pressure losses in HVAC duct fittings. *Applied Energy* 51: 233-248.

Ugursal, A., and Culp, C. 2007. Comparative analysis of CFDΔP vs. measured ΔP for compressed flexible ducts. *ASHRAE Transactions* 113(1): 462-469.

Table 1. Geometry of the Duct Fittings

Nominal Fitting Size, mm (in.) [A × a to C × c (Figure 2)]	Description
787 × 356 to 559 × 254 mm (31 × 14 to 22 × 10 in.)	Tee junction
787 × 356 to 559 × 254 mm (31 × 14 to 22 × 10 in.)	Lateral junction

Table 2. Inlet velocity and flow rate ratios for the four cases

Converging cases						Diverging cases	
Main velocity m/s (fpm)	Branch velocity m/s (fpm)	Q_b/Q_c	Main velocity m/s (fpm)	Branch velocity m/s (fpm)	Q_b/Q_c	Main velocity m/s (fpm)	Q_b/Q_c
20.3 (3996)	5.1(1004)	0.11	11.1 (2185)	20.3 (3996)	0.48	20.3 (3996)	0.1
17.1 (3366)	5.1(1004)	0.13	8.1 (1594)	17.1 (3366)	0.52	20.3 (3996)	0.15
20.3 (3996)	8.1 (1594)	0.17	8.1 (1594)	20.3 (3996)	0.56	20.3 (3996)	0.2
17.1 (3366)	8.1 (1594)	0.19	5.1 (1004)	14.1 (2776)	0.58	20.3 (3996)	0.3
20.3 (3996)	11.1 (2185)	0.22	5.1 (1004)	17.1 (3366)	0.631	17.1 (3366)	0.4
17.1 (3366)	11.1 (2185)	0.25	5.1 (1004)	20.3 (3996)	0.67	14.1 (2776)	0.5
17.1 (3366)	14.1 (2776)	0.29				14.1 (2776)	0.6
11.1 (2185)	11.1 (2185)	0.34				14.1 (2776)	0.7
14.1 (2776)	17.1 (3366)	0.38				11.1 (2185)	0.8
8.1 (1594)	11.1 (2185)	0.41				11.1 (2185)	0.85
5.1 (1004)	8.1 (1594)	0.45				11.1 (2185)	0.9

Q_b - flow rate of the branch section, Q_c - flow rate of the common section.

Table 3 Conditions for testing different surface roughnesses of the straight ducts

Case	1	3	Case	2	4
Main Velocity	11.1 m/s (2185 fpm)	11.1 m/s (2185 fpm)	Main Velocity	14.1 m/s (2776 fpm)	14.1 m/s (2776 fpm)
Branch velocity	8.1 m/s (1595 fpm)	8.1 m/s (1595 fpm)	Q_b / Q_c	0.1	0.2

Q_b - flow rate of the branch section, Q_c - flow rate of the common section

Table 4 The optimal surface roughness of the straight duct and turbulence model identified for the four cases specified by ASHRAE RP-1493

Case	Model	Surface roughness	Case	Model	Surface roughness
1	RSM	0.01	3	Standard k-ε	0.005
2	RSM	0.01	4	Standard k-ε	0.01

Table 5 Parameters for Equation (6)

Item	Parameter	Case 1)	Case 2)	Case 3)	Case 4)
C_b	y_0	1.20	1.46	0.54	0.73
	A	-1.25E+02	1.02E+02	-9.86E+01	1.07E+02
	R_0	-26.52	-15.16	-19.7	-17.63
C_s	y_0	0.32	0.16	0.34	0.30
	A	81.72	139.67	-220.82	174.54
	R_0	-6.56	-19.09	-11.67	-17.40

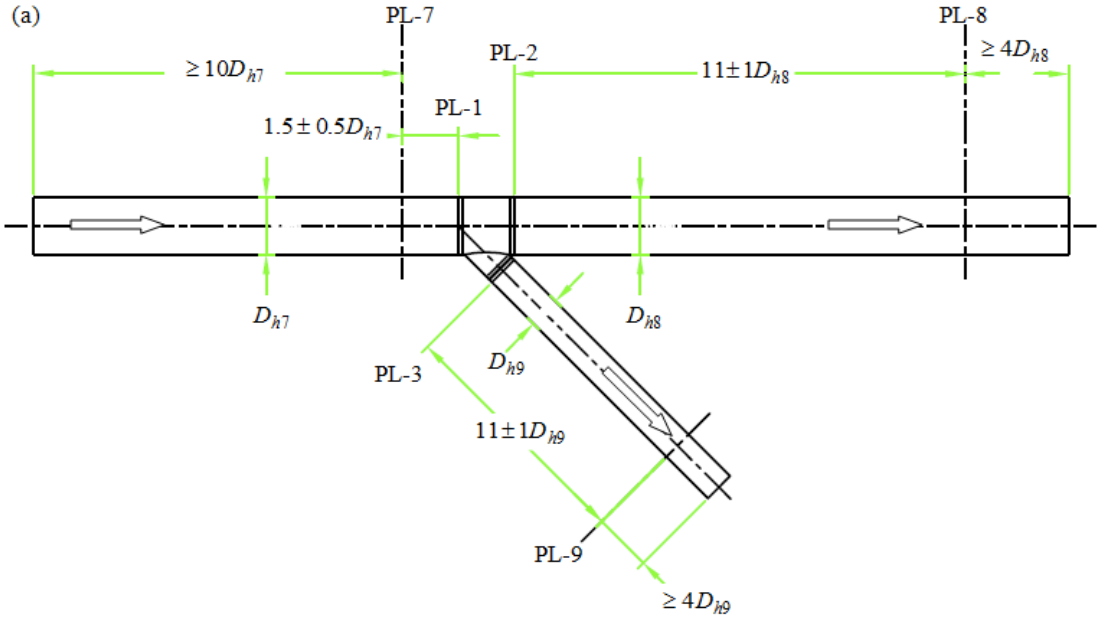

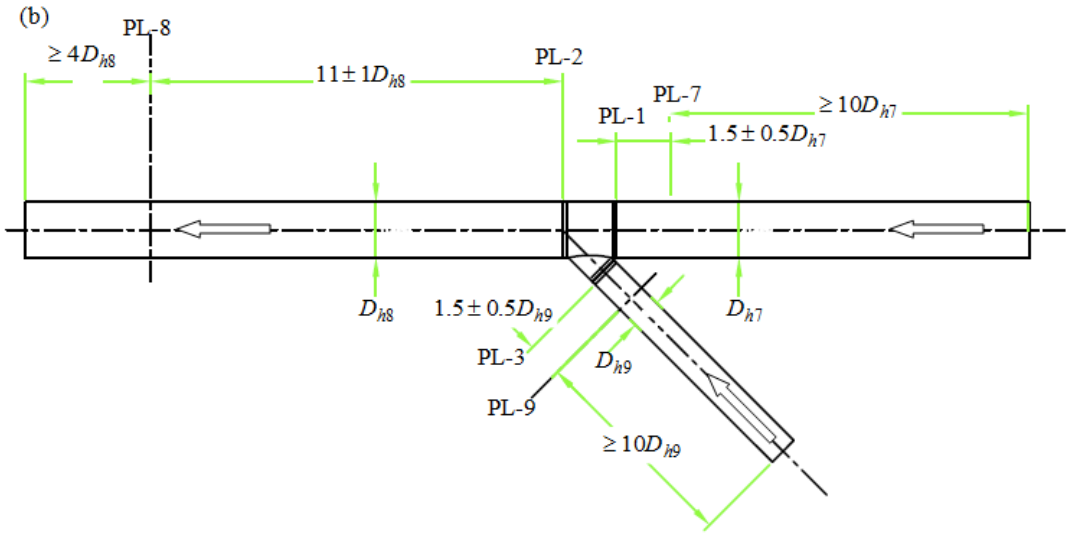

Figure 1 *(a) Diverging and (b) converging airflow test apparatus used by ASHRAE Standard 120*

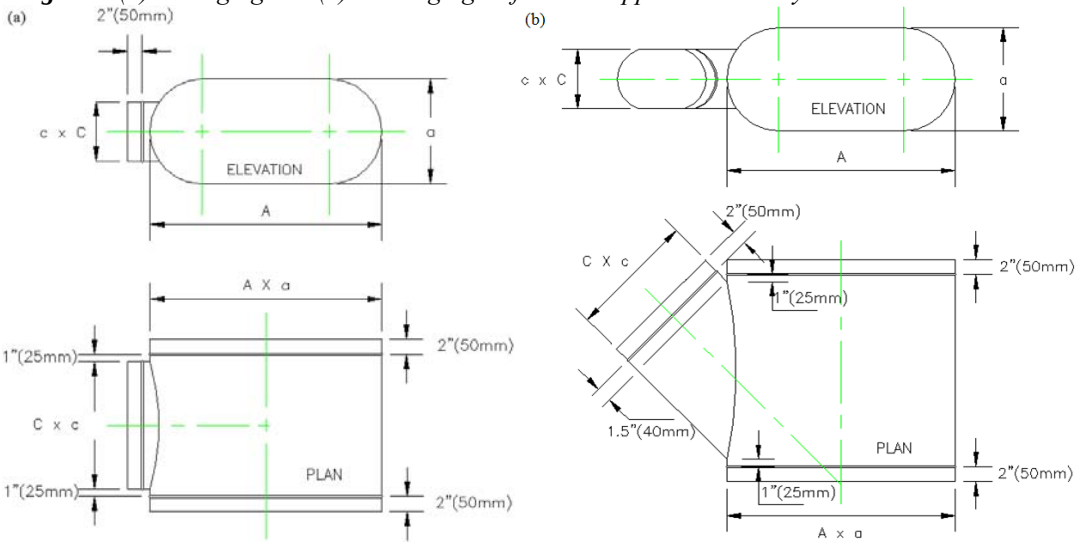

Figure 2 *(a) Flat oval straight body with tee junction and (b) flat oval straight body with lateral junction*

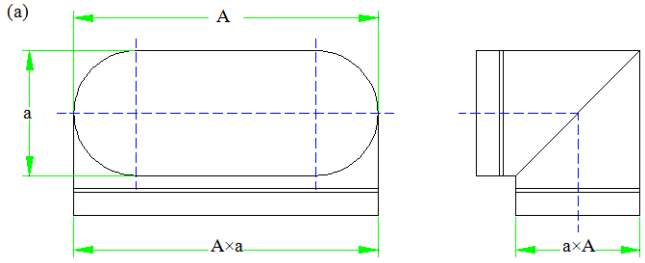

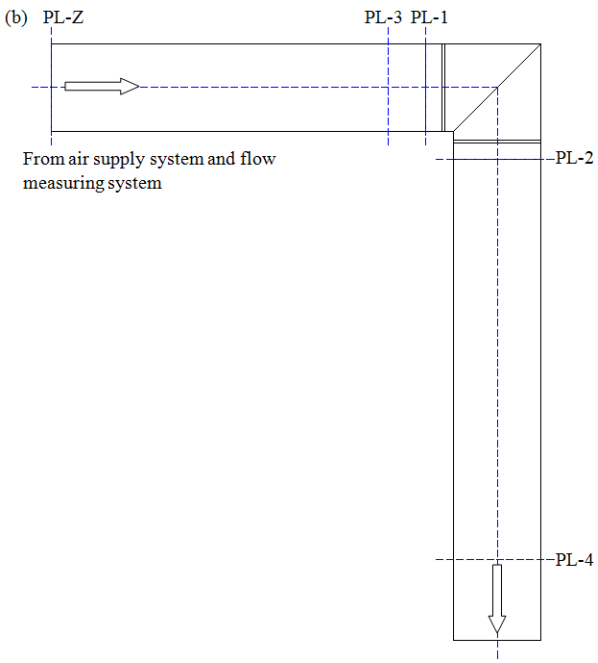

Figure 3 *(a) Mitered 90° easy bend elbow without vanes and (b) its simulation domain*

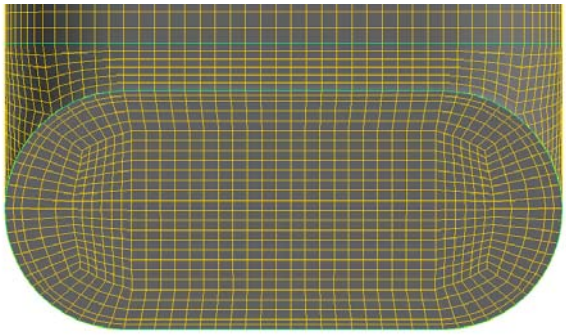

Figure 4 *The cell distribution for the elbow when most cell sizes were 10 mm*

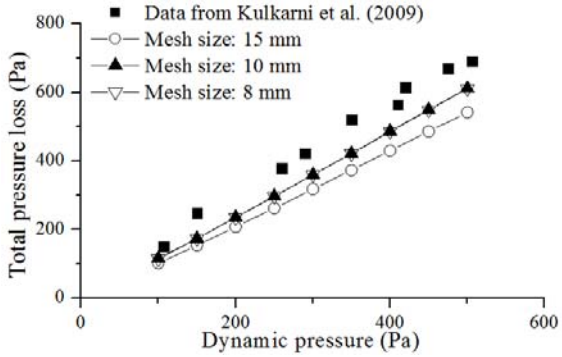

Figure 5 *Grid independence study for the elbow by using the RSM.*

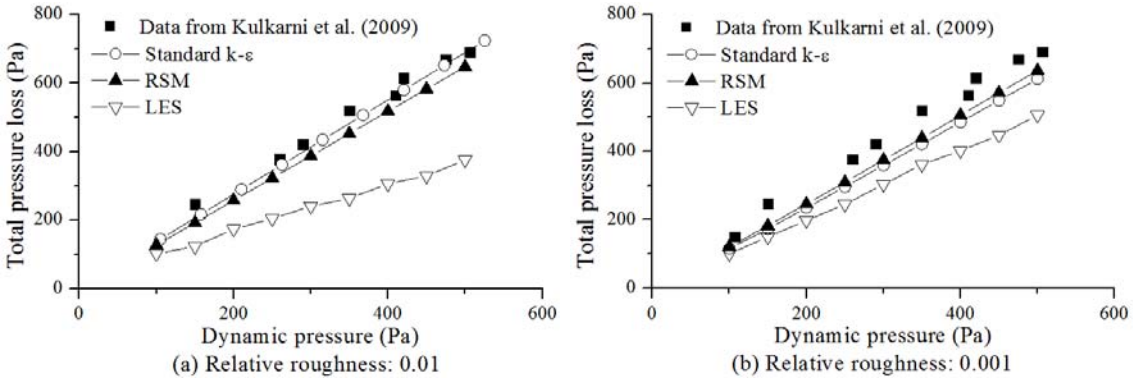

Figure 6 *Predicted pressure loss with different CFD models that had different flow rates at surface relative roughnesses of (a) 0.01 and (b) 0.001*

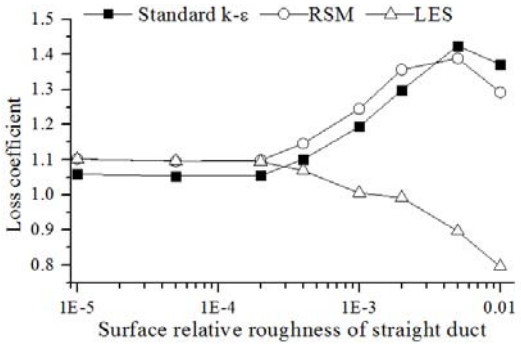

Figure 7 *The loss coefficient calculated with different surface relative roughnesses for an air velocity of 22.13 m/s (4356.3 fpm) in the elbow*

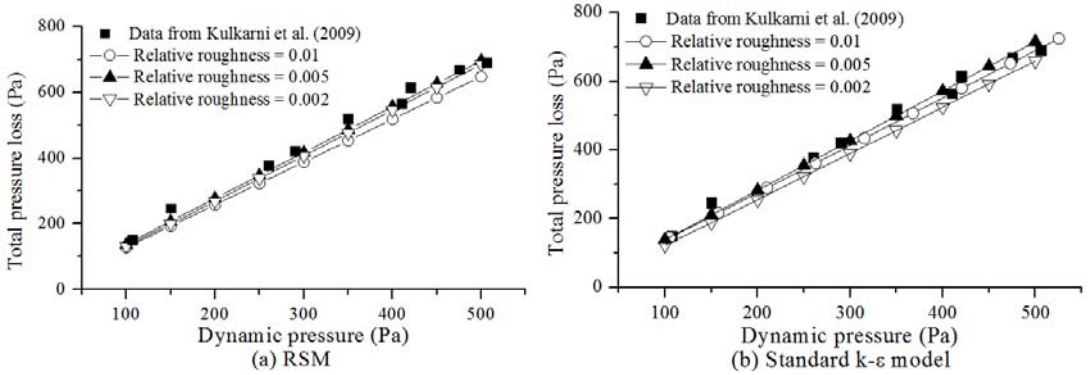

Figure 8 *Comparison of measured pressure loss coefficients for different air velocities with those calculated by (a) RSM and (b) the standard k-ε model under different surface roughnesses*

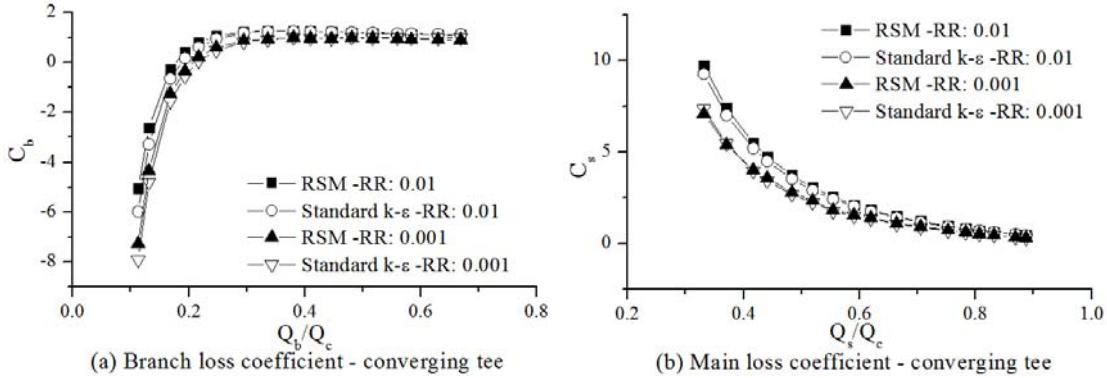

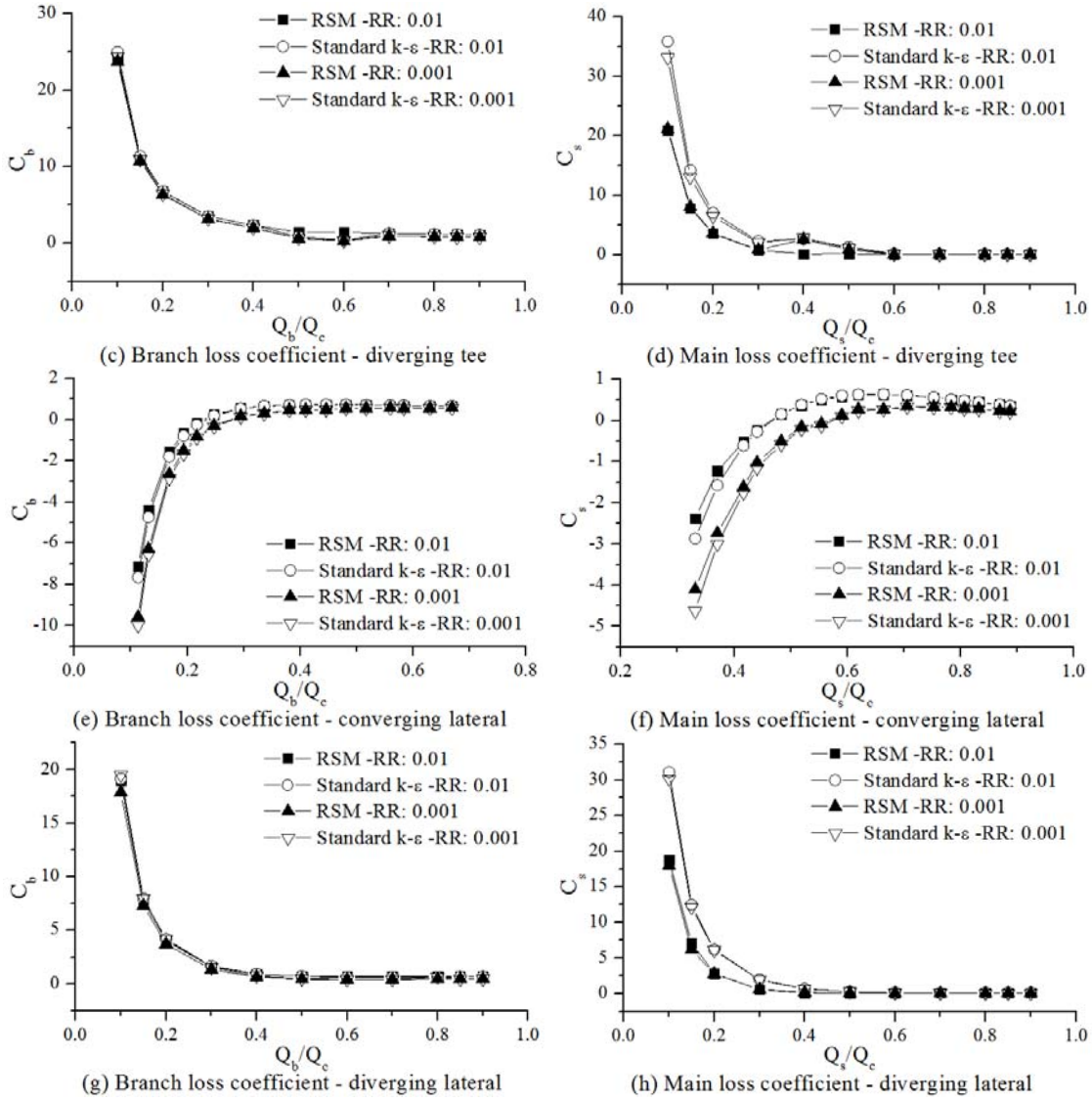

Figure 9 *Predicted pressure loss coefficients by the two CFD models under two different surface relative roughness values for the straight ducts (RR=relative roughness).*

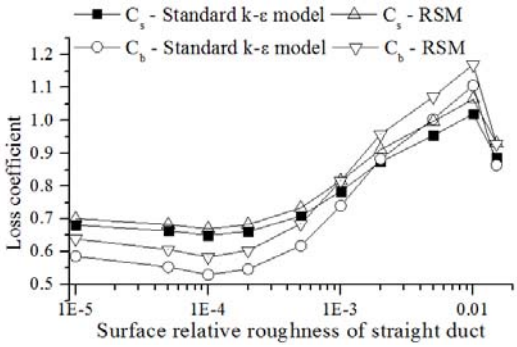

Figure 10 *Predicted loss coefficients with different roughnesses for the straight duct for Case 1.*

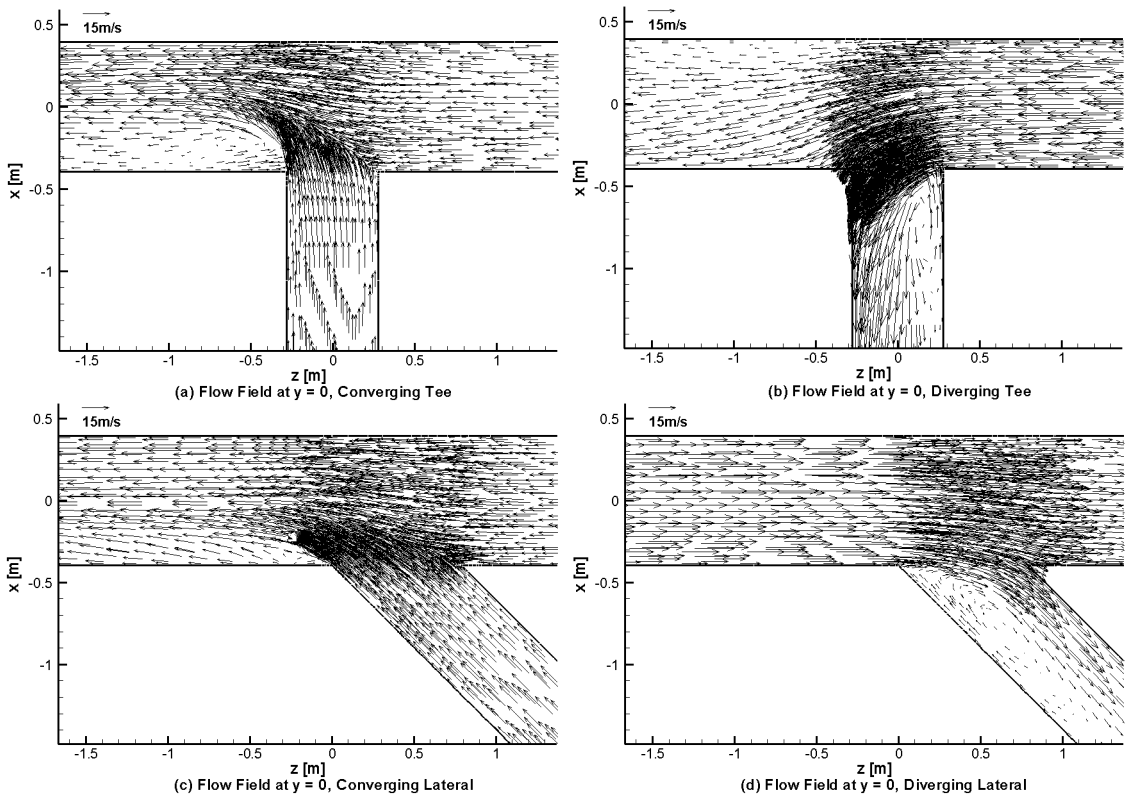

Figure 11 *Airflow patterns at the central cross section for the (a) converging tee, (b) diverging tee, (c) converging lateral, and (d) diverging lateral junctions*

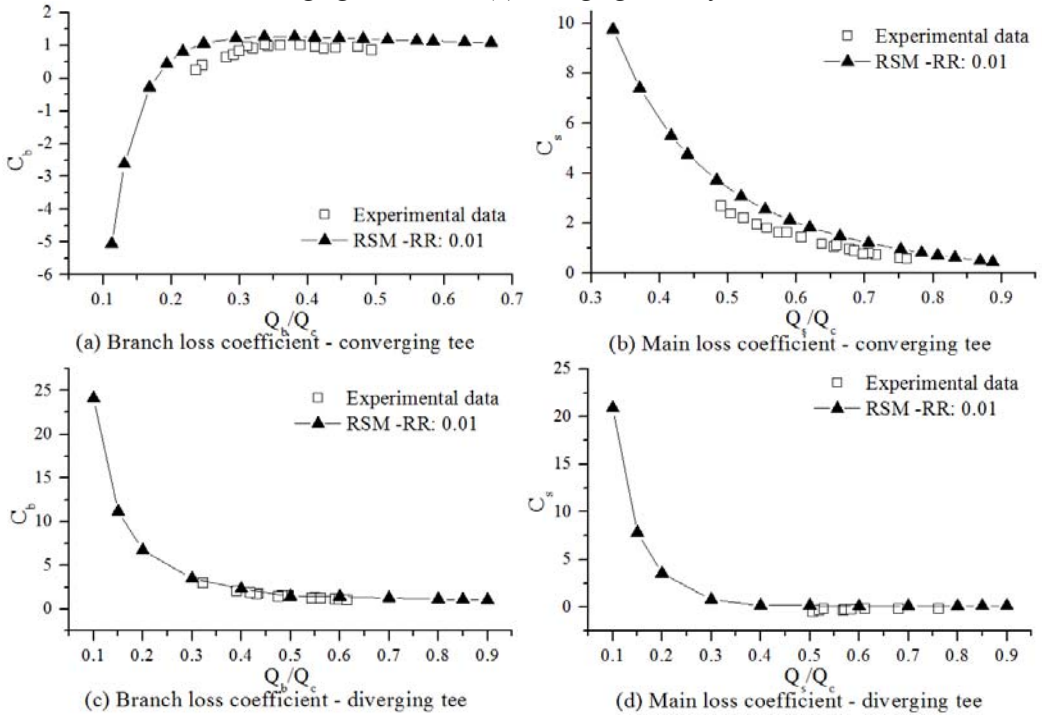

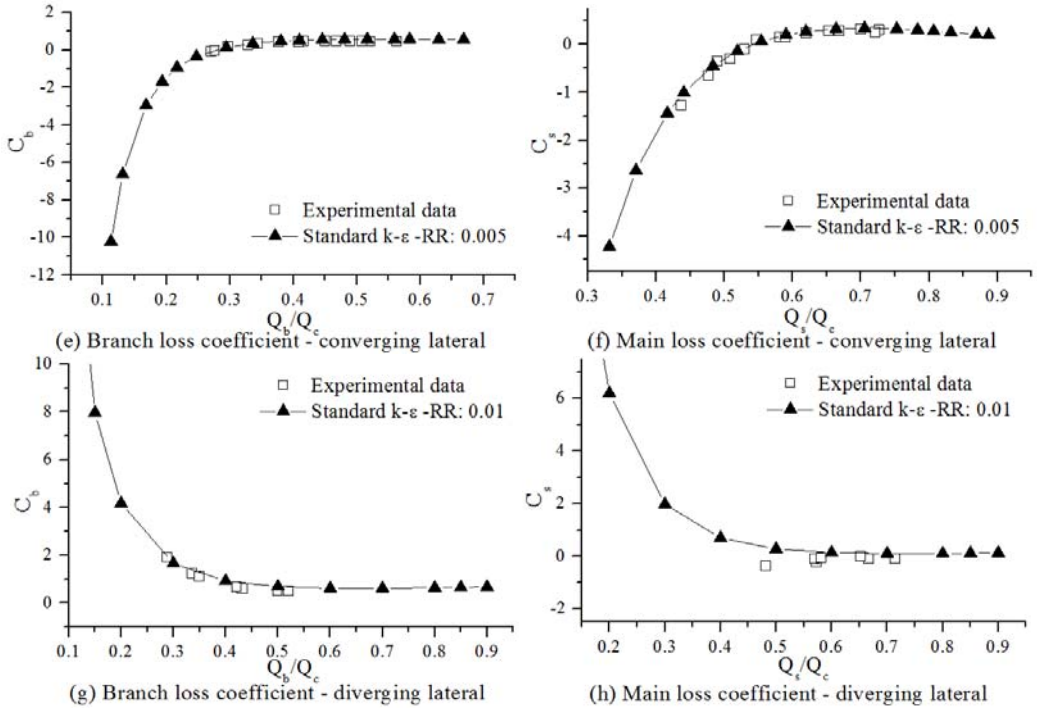

Figure 12 *Comparison of the predicted pressure loss coefficients for different flow rates with the experimental data provided by ASHRAE (RR stands for relative roughness, Experimental data was from ASHRAE)*